Astrodynamics Vol. 4, No. 3, 193–204, 2020 https://doi.org/10.1007/s42064-019-0057-x

Optimal solar sail transfers to circular Earth-synchronous displaced orbits

Alessandro A. Quarta (✉), Giovanni Mengali, and Marco Bassetto

Department of Civil and Industrial Engineering, University of Pisa, Pisa I-56122, Italy

ABSTRACT

The aim of this paper is to evaluate the minimum flight time of a solar sail-based spacecraft towards Earth-synchronous (heliocentric) circular displaced orbits. These are special displaced non-Keplerian orbits characterized by a period of one year, which makes them suitable for the observation of Earth's polar regions. The solar sail is modeled as a flat and purely reflective film with medium–low performance, that is, with a characteristic acceleration less than one millimeter per second squared. Starting from a circular parking orbit of radius equal to one astronomical unit, the optimal steering law is sought by considering the characteristic acceleration that is required for the maintenance of the target Earth-synchronous displaced orbit. The indirect approach used for the calculation of the optimal transfer trajectory allows the minimum flight time to be correlated with several Earth-synchronous displaced orbits, each one being characterized by given values of Earth–spacecraft distance and displacement over the ecliptic. The proposed mathematical model is validated by comparison with results available in the literature, in which a piecewise-constant steering law is used to find the optimal flight time for a transfer towards a one-year Type I non-Keplerian orbit.

KEYWORDS

solar sail

synchronous displaced orbit

trajectory optimization

Research Article

Received: 16 February 2019

Accepted: 4 May 2019

1 Introduction

Closed non-Keplerian orbits have attracted the scientific interest in recent years, due to their unique advantages in astronomical missions [1]. A very promising class is represented by displaced non-Keplerian orbits (DNKOs), which are so called because their orbital plane does not contain the primary body [2, 3]. These orbits require a continuous thrust to be maintained, in such a way that the centrifugal and gravitational forces acting on the spacecraft balance each other. A good approximation of a DNKO may be obtained through a sequence of Keplerian arcs patched by impulsive maneuvers, as has been proposed by McInnes [4] in the special case of DNKOs of circular shape, while a more general solution has been recently obtained by Caruso *et al.* [5] for approximating an elliptic DNKO with a sequence of azimuthally equally spaced impulses.

The propellant necessary to generate the required thrust limits the use of conventional propulsion systems (such as chemical or electric thruster) for those applications, and promotes the employment of propellantless propulsion systems, such as the photonic solar sail [6–9] or the more recent Electric Solar Wind Sail [10, 11]. In particular, DNKOs generated by solar sails have been proposed in mission applications both in heliocentric and planetocentric frameworks, as is discussed in the comprehensive survey by McKay *et al.* [1]. For example, Ceriotti *et al.* [12, 13] investigated the concept of a pole-sitter mission, in which the spacecraft is always above one of Earth's poles to obtain a continuous observation of zones with high geographic latitude. Also, Ceriotti and McInnes [14] proposed the use of doubly-symmetric, eight-shaped orbits in the Earth–Moon system for continuous coverage of the Earth's high-latitude zones. Heiligers *et al.* [15] investigated solar sail periodic orbits in the Earth–Moon circular restricted three-body

✉ a.quarta@ing.unipi.it

Nomenclature

$\boldsymbol{a}$	propulsive acceleration vector (mm/s^2)
a_c	characteristic acceleration (mm/s^2)
a_r, a_θ, a_γ	components of $\boldsymbol{a}$ in $\mathcal{T}_S$ (mm/s^2)
d	Earth–spacecraft distance (AU)
$\mathcal{D}$	spacecraft orbital plane
E	Earth's center-of-mass
$\mathcal{E}$	ecliptic plane
H	distance between plane $\mathcal{E}$ and plane $\mathcal{D}$ (AU)
$\mathcal{H}$	Hamiltonian function
$\mathcal{H}_c$	part of Hamiltonian function that depends on the controls
$\hat{\boldsymbol{i}}$, $\hat{\boldsymbol{j}}$, $\hat{\boldsymbol{k}}$	unit vectors of $\mathcal{T}$
J	performance index
$\hat{\boldsymbol{n}}$	unit vector normal to the sail plane
N	number of control segments
O	Sun's center-of-mass
O'	displaced orbit center
$\mathcal{P}$	plane passing through $\{O, O', E\}$
$\hat{\boldsymbol{p}}_r$, $\hat{\boldsymbol{p}}_\theta$, $\hat{\boldsymbol{p}}_\gamma$	unit vectors of $\mathcal{T}_S$
$\boldsymbol{r}$	Sun–sail vector, with $r \triangleq \|\boldsymbol{r}\|$ (AU)
$r_\oplus$	Sun–Earth reference distance (AU)
S	spacecraft center-of-mass
t	time (days)
t_f	total flight time (days)
T	orbital period (days)
$T_\oplus$	Earth's orbital period (days)
v_r, v_θ, v_γ	components of spacecraft inertial velocity in $\mathcal{T}_S$ (km/s)
$\{x, y, z\}$	axes of $\mathcal{T}$
α	cone angle (rad)
β	lightness number
γ	elevation angle (rad)
δ	clock angle (rad)
θ	polar angle (rad)
$\boldsymbol{\lambda}$	Lawden's primer vector, with $\boldsymbol{\lambda} \triangleq [\lambda_{v_r}, \lambda_{v_\theta}, \lambda_{v_\gamma}]^T$
λ_i	variables adjoint to the ith state
$\mu_\odot$	Sun's gravitational parameter (km^3/s^2)
ρ	non-Keplerian orbit radius (AU)
$\mathcal{T}$	heliocentric-ecliptic reference frame
$\mathcal{T}_S$	spherical reference frame
ω	spacecraft angular velocity (rad/s)
$\omega_\oplus$	Earth's angular velocity (rad/s)
Subscripts	
d	required
λ	referred to $\boldsymbol{\lambda}$
0	initial
Superscripts	
$\sim$	dimensionless
$\star$	optimal
$\cdot$	time derivative
$\wedge$	unit vector

problem for the observation of the polar regions of the two bodies. Ozimek *et al.* [16] studied potential orbits for continuous surveillance of the Moon's south pole with a single solar sail-based spacecraft, and Wawrzyniak and Howell [17] proposed to use solar sails as a communication relay for a base at the lunar south pole. In a heliocentric framework, Heiligers and Scheeres [18] analyzed the possibility of employing a solar sail to generate artificial equilibrium points and displaced periodic orbits around asteroids or binary asteroid systems. Moreover, an attractive application is represented by an Earth–Mars interplanetary communication relay [19] in support of

crewed missions to Mars. Other applications include solar wind monitoring [20], and real-time stereographic investigations of a planetary surface [21–23]. Similar applications have been studied also using an Electric Solar Wind Sail as primary propulsion system [24, 25] and in the context of formation flying control design.

Of particular interest are those orbits with a period equal to 1 year and whose orbital plane is parallel to the ecliptic plane. These DNKOs are useful for the aim of observing the polar regions of the Earth and, to maximize their effectiveness, it is important that the spacecraft angular position matches that of our planet, in such a way that the spacecraft and the Earth move synchronously at a (roughly) constant distance [26]. For that reason, and according to the nomenclature adopted by Powers and Coverstone [27], such a special kind of non-Keplerian orbits is here referred to as Earth-synchronous displaced orbit (ESDO). Assuming a circular Earth's heliocentric orbit, the required solar sail (reference) propulsive acceleration (or the sail lightness number) may be found as a function of the displaced orbit radius and the displacement relative to the ecliptic [2]. The aim of this paper is to address the problem of calculating the minimum flight time required to reach a heliocentric circular ESDO by considering a spacecraft whose primary propulsion system is a medium–low performance ideal solar sail. This problem was first discussed by Hughes and McInnes [28], who obtained some interesting results with a direct optimization method, combining a genetic approach with a sequential quadratic programming algorithm. In their analysis [28], the spacecraft trajectory was divided into a given finite number of arcs with equal duration. In particular, within each arc the sail attitude has been held constant in a typical orbital reference frame, in order to obtain a simpler expression of the spacecraft thrust vector.

Even though optimal transfers to ESDOs are a challenging problem due to their nonintuitive nature [28], the approach suggested in this paper uses an indirect method, which allows a global minimum solution to be found for a number of ESDOs, with different values of orbit radius and displacement. The optimal steering law gives a continuous variation of the thrust vector control angles (that is, the cone and clock angles), and the obtained solutions show substantial improvements with respect to the literature results [28]. Moreover, the knowledge of the truly optimal solution offers also an useful benchmark when the continuous steering law is approximated by means of a prescribed (and discrete) number of thrust vector directions [29]. In that case, a piecewise-constant steering law is the least complex law possible, though the instantaneous changes in the sail orientation is still disadvantageous from the attitude control point of view.

2 Problem description

Consider a solar sail-based spacecraft S, which initially covers a circular ecliptic orbit of radius $r_\oplus \triangleq 1\,\mathrm{AU}$ and period $T_\oplus \triangleq 2\pi\sqrt{r_\oplus^3/\mu_\odot} = 1\,\mathrm{year}$, where $\mu_\odot$ is the Sun's gravitational parameter. This situation is representative of a sail deployment just outside the Earth's sphere of influence, when the spacecraft leaves the planet with zero hyperbolic excess speed and the Earth's heliocentric orbit eccentricity is neglected. Introduce a heliocentric-ecliptic (inertial) reference frame $\mathcal{T}(O; x, y, z)$ centered at the Sun's center-of-mass O, with unit vectors $\hat{\boldsymbol{\imath}}$, $\hat{\boldsymbol{\jmath}}$, and $\hat{\boldsymbol{k}}$. The plane (x, y) contains the circular parking orbit, $\hat{\boldsymbol{\imath}}$ points to the vernal equinox, and $\hat{\boldsymbol{k}}$ points to the north ecliptic pole; see Fig. 1 in which $\mathcal{E}$ is the ecliptic. Assume a flat sail and an ideal force model [30] without degradation [31], that is, an ideal rigid mirror characterized by a full and specular reflection of the incident light. In this simplified case, the spacecraft propulsive acceleration vector is [32]:

$$\boldsymbol{a} = a_\mathrm{c}\left(\frac{r_\oplus}{r}\right)^2 \cos^2\alpha\,\hat{\boldsymbol{n}} \tag{1}$$

where r is the Sun–spacecraft distance, $\hat{\boldsymbol{n}}$ is the unit vector normal to the sail nominal plane in the direction opposite to the Sun, $\alpha \in [0, \pi/2]\,\mathrm{rad}$ is the (cone) angle between the Sun–spacecraft line and the direction of $\hat{\boldsymbol{n}}$, and a_c is the spacecraft characteristic acceleration, defined as the maximum propulsive acceleration magnitude $\|\boldsymbol{a}\|$ (obtained with a Sun-facing sail with $\alpha = 0$) at a reference Sun–spacecraft distance of 1 AU; see Fig. 1.

The spacecraft mission is to reach a circular non-Keplerian orbit of radius $\rho < r_\oplus$ and period $T = T_\oplus$, whose orbital plane $\mathcal{D}$ is displaced at a distance H relative to the ecliptic $\mathcal{E}$; see Fig. 2. Also, O' is the displaced orbit center that coincides with the point of intersection between the plane $\mathcal{D}$ and the z-axis. The spacecraft covers the circular displaced orbit with a constant angular velocity $\omega = 2\pi/T$, which matches

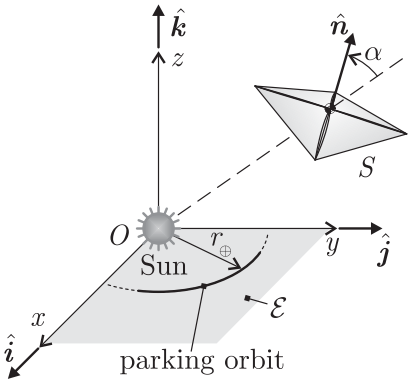

Fig. 1 Inertial reference frame $\mathcal{T}(O; x, y, z)$ and sail cone angle α.

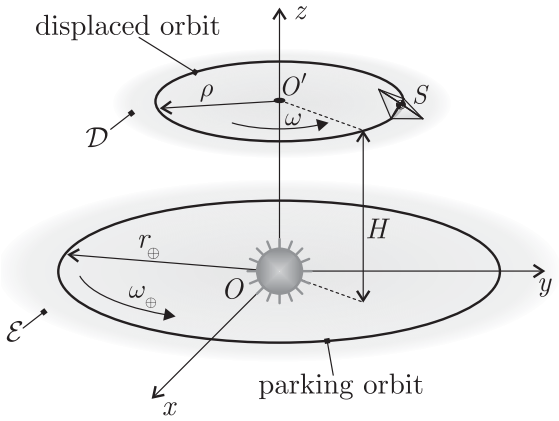

Fig. 2 Conceptual scheme of heliocentric circular displaced orbit.

that of Earth along its heliocentric orbit, i.e., $\omega = \omega_\oplus = \sqrt{\mu_\odot / r_\oplus^3} \simeq 0.986\,\mathrm{deg/day}$.

In particular, at the end of the transfer, the spacecraft must belong to the plane $\mathcal{P}$ that contains the z-axis, the origin O, and the Earth's center-of-mass E; see Fig. 3. The final (ESDO type) orbit is a special case of the so called Type I non-Keplerian orbits [32], which gives the minimum distance between the spacecraft and the Earth's center-of-mass E. In particular, the minimum Earth–spacecraft distance d may be written in a dimensionless form as

$$\widetilde{d} \triangleq \frac{d}{r_\oplus} = \sqrt{\widetilde{H}^2 + (1-\widetilde{\rho})^2} \tag{2}$$

where $\{\widetilde{H}, \widetilde{\rho}\}$ are the dimensionless values of $\{H, \rho\}$, that is

$$\widetilde{H} \triangleq \frac{H}{r_\oplus}, \qquad \widetilde{\rho} \triangleq \frac{\rho}{r_\oplus} < 1 \tag{3}$$

For a given pair $\{H, \rho\}$, the solar sail performance (in terms of characteristic acceleration and sail cone angle)

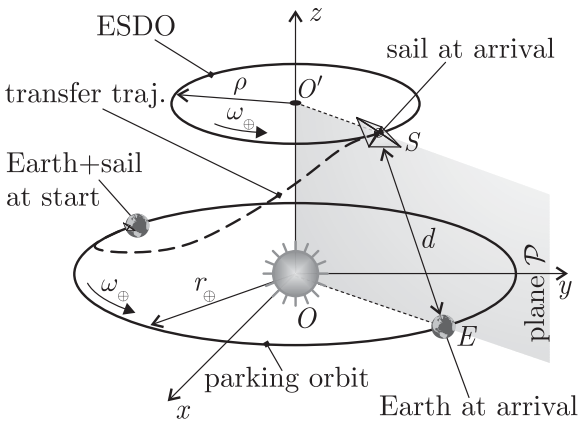

Fig. 3 Earth-synchronous displaced orbit concept.

required to maintain the ESDO depends on the thermo-optical characteristics of the reflective film. More precisely, the characteristic acceleration a_{c_d} necessary for an ideal sail can be obtained by adapting the equation proposed by McInnes [32], viz.

$$a_{c_d} = \frac{\mu_\odot}{r_\oplus^2} \sqrt{1 + \left(\widetilde{H}/\widetilde{\rho}\right)^2} \times \frac{\sqrt{\left\{\left(\widetilde{H}/\widetilde{\rho}\right)^2 + \left[1 - \sqrt{(\widetilde{H}^2 + \widetilde{\rho}^2)^3}\right]^2\right\}^3}}{\left[\left(\widetilde{H}/\widetilde{\rho}\right)^2 + 1 - \sqrt{(\widetilde{H}^2 + \widetilde{\rho}^2)^3}\right]^2} \tag{4}$$

while the required sail cone angle α_d has a constant value given by [32]:

$$\tan\alpha_d = \frac{\left(\widetilde{H}/\widetilde{\rho}\right)\sqrt{\left(\widetilde{H}^2 + \widetilde{\rho}^2\right)^3}}{\left(\widetilde{H}/\widetilde{\rho}\right)^2 + 1 - \sqrt{(\widetilde{H}^2 + \widetilde{\rho}^2)^3}} \tag{5}$$

Actually, the original expressions obtained by McInnes [32] are given in terms of sail lightness number $\beta = \beta_d$, which, for an ideal sail, can be written as a function of the characteristic acceleration as

$$\beta \triangleq \frac{a_c}{\mu_\odot / r_\oplus^2} \tag{6}$$

with $\mu_\odot / r_\oplus^2 \simeq 5.93\,\mathrm{mm/s^2}$. The level curves $a_{c_d} = a_{c_d}(\widetilde{H}, \widetilde{\rho})$ and $\alpha_d = \alpha_d(\widetilde{H}, \widetilde{\rho})$, given by Eqs. (4) and (5), are drawn in Fig. 4 for a medium–low performance solar sail, that is, for a sail with a characteristic acceleration less than $1\,\mathrm{mm/s^2}$. In particular, Fig. 4 shows both the Earth–spacecraft dimensionless distance $\widetilde{d}$ given by Eq. (2), and the Earth's sphere of influence (SOI), whose dimensionless radius is roughly $\widetilde{d} = 0.01$. Note that

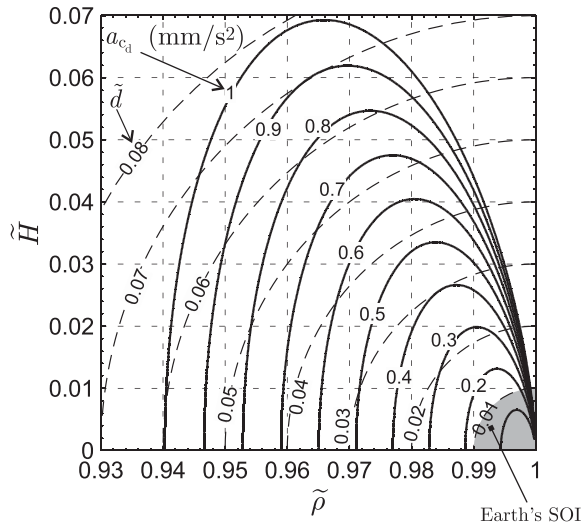

(a) Characteristic acceleration

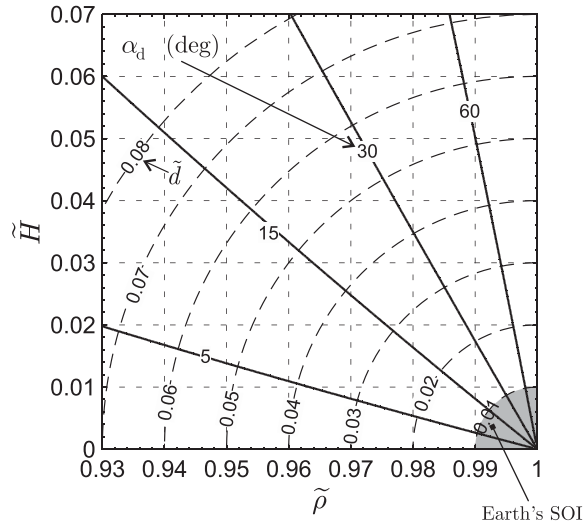

(b) Sail cone angle

Fig. 4 Solar sail required performance $\{a_{c_d}, \alpha_d\}$ and Earth–spacecraft dimensionless distance $\tilde{d}$ as a function of ESDO characteristics $\{\tilde{H}, \tilde{\rho}\}$.

a maximum displacement over the ecliptic of about $H = 0.07$ AU can be obtained with a solar sail of $a_c = 1\,\mathrm{mm/s^2}$, while assuming $a_c = 0.3\,\mathrm{mm/s^2}$, the maximum value of H is roughly 0.02 AU. When $a_c < 0.135\,\mathrm{mm/s^2}$, the spacecraft falls inside the Earth's SOI, and Eqs. (4) and (5) cannot be used to model the required solar sail performance to cover an ESDO.

2.1 Equations of motion

The solar sail-based heliocentric motion during the transfer phase is analyzed in a spherical reference frame $\mathcal{T}_S(O; r, \theta, \gamma)$ of unit vector $\hat{\boldsymbol{p}}_r$, $\hat{\boldsymbol{p}}_\theta$, and $\hat{\boldsymbol{p}}_\gamma$ defined as

$$\hat{\boldsymbol{p}}_r = \hat{\boldsymbol{r}} \triangleq \boldsymbol{r}/r, \quad \hat{\boldsymbol{p}}_\theta = \frac{\hat{\boldsymbol{k}} \times \hat{\boldsymbol{r}}}{\left\| \hat{\boldsymbol{k}} \times \hat{\boldsymbol{r}} \right\|}, \quad \hat{\boldsymbol{p}}_\gamma = \hat{\boldsymbol{p}}_r \times \hat{\boldsymbol{p}}_\theta \tag{7}$$

where $\boldsymbol{r}$ is the Sun–spacecraft position vector. In particular, $\theta \in [0, 2\pi)$ rad is the polar angle measured counterclockwise from the x-axis (vernal equinox direction), and $\gamma \in [-\pi/2, \pi/2]$ rad is the elevation angle relative to the ecliptic plane; see Fig. 5.

According to Ref. [33], the spacecraft equations of motion in the spherical reference frame are

$$\dot{r} = v_r \tag{8}$$

$$\dot{\theta} = \frac{v_\theta}{r \cos\gamma} \tag{9}$$

$$\dot{\gamma} = \frac{v_\gamma}{r} \tag{10}$$

$$\dot{v}_r = \frac{v_\theta^2 + v_\gamma^2}{r} - \frac{\mu_\odot}{r^2} + a_r \tag{11}$$

$$\dot{v}_\theta = \frac{v_\theta\, v_\gamma \tan\gamma - v_r\, v_\theta}{r} + a_\theta \tag{12}$$

$$\dot{v}_\gamma = -\frac{v_\theta^2 \tan\gamma + v_r\, v_\gamma}{r} + a_\gamma \tag{13}$$

where $\{v_r, v_\theta, v_\gamma\}$ are the components of the spacecraft inertial velocity in $\mathcal{T}_S$, and $\{a_r, a_\theta, a_\gamma\}$ are the components of $\boldsymbol{a}$ in $\mathcal{T}_S$. The latter, with the aid of Eq. (1) and Fig. 6, may be written as a function of the sail cone angle α and clock angle $\delta \in [0, 2\pi)$ rad as

$$a_r = a_c \left(\frac{r_\oplus}{r}\right)^2 \cos^3\alpha \tag{14}$$

$$a_\theta = a_c \left(\frac{r_\oplus}{r}\right)^2 \cos^2\alpha \sin\alpha \cos\delta \tag{15}$$

$$a_\gamma = a_c \left(\frac{r_\oplus}{r}\right)^2 \cos^2\alpha \sin\alpha \sin\delta \tag{16}$$

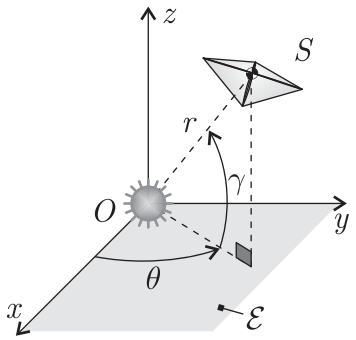

Fig. 5 Spherical (heliocentric) reference frame $\mathcal{T}_S(O; r, \theta, \gamma)$.

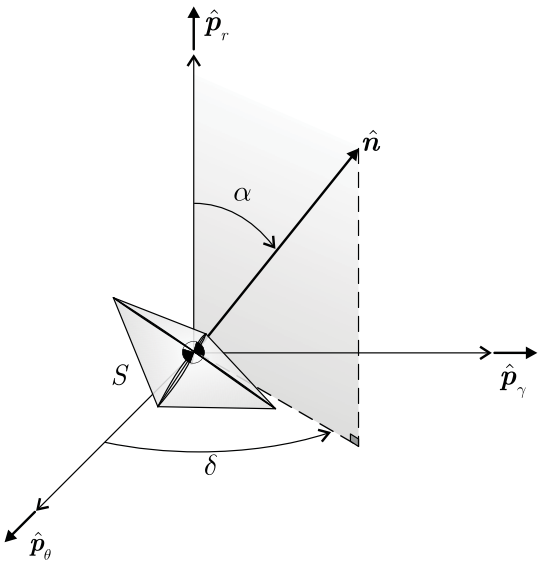

Fig. 6 Ideal solar sail thrust vector control angles $\{\alpha, \delta\}$.

Because the spacecraft initially covers a circular ecliptic orbit of radius $r_\oplus$ around the Sun, Eqs. (8)–(13) are completed by the initial conditions (at time $t_0 \triangleq 0$)

$$\begin{aligned} &r(t_0) = r_\oplus, \quad \theta(t_0) = \gamma(t_0) = 0, \\ &v_r(t_0) = v_\gamma(t_0) = 0, \quad v_\theta(t_0) = \sqrt{\tfrac{\mu_\odot}{r_\oplus}} \end{aligned} \tag{17}$$

where, for symmetry reasons, the polar angle $\theta(t_0)$ is set equal to zero without loss of generality.

For a given control law $\alpha = \alpha(t)$ and $\delta = \delta(t)$, with $t \in [t_0, t_\mathrm{f}]$ (where t_f is the total flight time), the time variation of the propulsive acceleration components are given by Eqs. (14)–(16) and the transfer trajectory is obtained by numerical integration of Eqs. (8)–(13) with initial conditions (17). The control law analysis and design is discussed in the next section.

2.2 Trajectory optimization

The solar sail trajectory is now analyzed in an optimal framework, by minimizing the flight time t_f required to transfer the vehicle from the circular parking orbit to the final circular ESDO of given characteristics $\{H, \rho\}$ (or $\{\widetilde{H}, \widetilde{\rho}\}$). Note that, in this case, the spacecraft characteristic acceleration is obtained from Eq. (4) by enforcing the condition $a_\mathrm{c} = a_{\mathrm{c_d}}$, which allows the spacecraft to cover the target ESDO. On the other hand, a value of $a_\mathrm{c} > a_{\mathrm{c_d}}(\widetilde{H}, \widetilde{\rho})$ could theoretically be selected with the aim to reduce the flight time. Nevertheless, a value of the characteristic acceleration greater than $a_{\mathrm{c_d}}$ would imply a reduction of a_c over the target ESDO which, in its turn, could be obtained by covering part of the sail surface with a set of electrochromic panels [34, 35], or through variations in the sail area [36, 37].

The trajectory optimization problem consists in finding $\alpha = \alpha(t)$ and $\delta = \delta(t)$ that maximize the performance index:

$$J \triangleq -t_\mathrm{f} \tag{18}$$

with an indirect approach. The Hamiltonian function $\mathcal{H}$ is

$$\begin{aligned} \mathcal{H} =& \lambda_r\, v_r + \lambda_\theta \frac{v_\theta}{r\,\cos\gamma} + \lambda_\gamma \frac{v_\gamma}{r} + \lambda_{v_r}\left(\frac{v_\theta^2+v_\gamma^2}{r} - \frac{\mu_\odot}{r^2}\right) \\ &+ \lambda_{v_\theta}\frac{v_\theta\, v_\gamma\, \tan\gamma - v_r\, v_\theta}{r} - \lambda_{v_\gamma}\frac{v_\theta^2\, \tan\gamma + v_r\, v_\gamma}{r} + \mathcal{H}_\mathrm{c} \end{aligned} \tag{19}$$

where $\{\lambda_r, \lambda_\theta, \lambda_\gamma, \lambda_{v_r}, \lambda_{v_\theta}, \lambda_{v_\gamma}\}$ is the set of variables adjoint to the states $\{r, \theta, \gamma, v_r, v_\theta, v_\gamma\}$, whose time derivatives are given by the Euler–Lagrange equations:

$$\begin{aligned} &\dot{\lambda}_r = -\frac{\partial \mathcal{H}}{\partial r}, \quad \dot{\lambda}_\theta = -\frac{\partial \mathcal{H}}{\partial \theta}, \\ &\dot{\lambda}_\gamma = -\frac{\partial \mathcal{H}}{\partial \gamma}, \quad \dot{\lambda}_{v_r} = -\frac{\partial \mathcal{H}}{\partial v_r}, \\ &\dot{\lambda}_{v_\theta} = -\frac{\partial \mathcal{H}}{\partial v_\theta}, \quad \dot{\lambda}_{v_\gamma} = -\frac{\partial \mathcal{H}}{\partial v_\gamma} \end{aligned} \tag{20}$$

The whole expression of the Euler–Lagrange equations is here omitted for the sake of conciseness, but their calculation is straightforward. In Eq. (19), the term $\mathcal{H}_\mathrm{c}$ is that portion of the Hamiltonian function that depends on the thrust vector control angles $\{\alpha, \delta\}$, see also Eqs. (14)–(16), viz.

$$\begin{aligned} \mathcal{H}_\mathrm{c} \triangleq a_\mathrm{c}\left(\frac{r_\oplus}{r}\right)^2 \cos^2\alpha (&\lambda_{v_r}\,\cos\alpha + \lambda_{v_\theta}\,\sin\alpha\,\cos\delta \\ &+ \lambda_{v_\gamma}\,\sin\alpha\,\sin\delta) \end{aligned} \tag{21}$$

According to Pontryagin's maximum principle [38], the optimal control law $\alpha = \alpha^\star(t)$ and $\delta = \delta^\star(t)$ is obtained by maximizing, at each time $t \in [t_0, t_\mathrm{f}]$, the function $\mathcal{H}_\mathrm{c}$ in Eq. (21). It may be verified that the optimal cone and clock angles coincide with the classical Sauer's result [39], viz.

$$\sin\delta^\star = \frac{\lambda_{v_\gamma}}{\sqrt{\lambda_{v_r}^2 + \lambda_{v_\theta}^2 + \lambda_{v_\gamma}^2}}, \quad \cos\delta^\star = \frac{\lambda_{v_\theta}}{\sqrt{\lambda_{v_r}^2 + \lambda_{v_\theta}^2 + \lambda_{v_\gamma}^2}} \tag{22}$$

$$\tan\alpha^\star = \frac{\sqrt{8 + \cos^2\alpha_\lambda} - 3\,\cos\alpha_\lambda}{4\sin\alpha_\lambda} \tag{23}$$

where $\alpha_\lambda \in [0, \pi]$ rad is the cone angle of Lawden's primer vector [40] $\boldsymbol{\lambda} \triangleq [\lambda_{v_r}, \lambda_{v_\theta}, \lambda_{v_\gamma}]^{\mathrm{T}}$, that is

$$\alpha_\lambda \triangleq \arccos\left(\frac{\lambda_{v_r}}{\sqrt{\lambda_{v_r}^2 + \lambda_{v_\theta}^2 + \lambda_{v_\gamma}^2}}\right) \tag{24}$$

Note that Eq. (22) can be rewritten in a more compact form by introducing the primer vector clock angle δ_λ defined as

$$\sin\delta_\lambda = \frac{\lambda_{v_\gamma}}{\sqrt{\lambda_{v_r}^2 + \lambda_{v_\theta}^2 + \lambda_{v_\gamma}^2}}, \quad \cos\delta_\lambda = \frac{\lambda_{v_r}^2 + \lambda_{v_\theta}}{\sqrt{\lambda_{v_r}^2 + \lambda_{v_\theta}^2 + \lambda_{v_\gamma}^2}} \tag{25}$$

in such a way that Eq. (22) reduce to

$$\delta^\star = \delta_\lambda \tag{26}$$

which states that $\hat{\boldsymbol{\lambda}} \triangleq \boldsymbol{\lambda}/\|\boldsymbol{\lambda}\|$, $\hat{\boldsymbol{r}}$, and $\hat{\boldsymbol{n}}$ belong to the same plane [41, 42]; see Fig. 7.

The optimal control law $\alpha^\star = \alpha^\star(\alpha_\lambda)$, given by Eq. (23), is shown in Fig. 8.

Finally, the two-point boundary value problem (TPBVP) associated with the optimization problem is completed by the following constraints at the (unknown) final time t_f:

$$\begin{aligned}
&r(t_\mathrm{f}) = r_\oplus\sqrt{\widetilde{H}^2 + \widetilde{\rho}^2}, \quad \theta(t_\mathrm{f}) = \omega_\oplus\, t_\mathrm{f},\\
&\gamma(t_\mathrm{f}) = \arctan\left(\frac{\widetilde{H}}{\widetilde{\rho}}\right),\\
&v_r(t_\mathrm{f}) = v_\gamma(t_\mathrm{f}) = 0, \quad v_\theta(t_\mathrm{f}) = \widetilde{\rho}\sqrt{\frac{\mu_\odot}{r_\oplus}},\\
&\mathcal{H}(t_\mathrm{f}) = 1 + \omega_\oplus\,\lambda_\theta(t_\mathrm{f})
\end{aligned} \tag{27}$$

where the last relation comes from the transversality condition [43]. The TPBVP has been solved by means of a hybrid numerical technique that uses global optimization techniques to obtain a first guess of the adjoint variables, while the solution is then refined with gradient-based and direct methods [41]. The differential Eqs. (8)–(13) and Eq. (20) have been integrated in double precision using a variable order Adams–Bashforth–Moulton solver scheme [44] with absolute and relative errors of 10^{-12}.

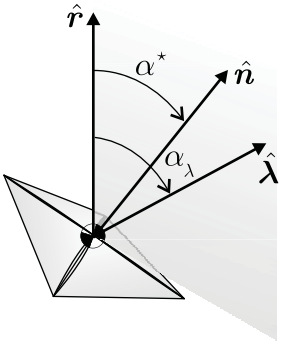

Fig. 7 Optimal configuration of $\hat{\boldsymbol{\lambda}}$, $\hat{\boldsymbol{r}}$, and $\hat{\boldsymbol{n}}$.

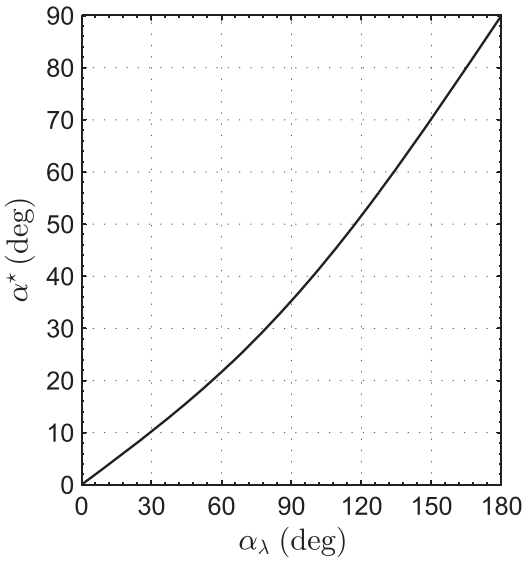

Fig. 8 Optimal sail cone angle $\alpha^\star$ as a function of the primer vector cone angle α_λ.

3 Numerical simulations

The previous procedure for calculating the optimal transfer to displaced orbits has been validated with results taken from the literature. More precisely, the simulations have been compared with the results obtained by Hughes and McInnes [28] with a hybrid optimization method in which the optimal time-variation of the control angles is approximated through a piecewise-constant steering law with N equally-spaced control segments. In particular, Ref. [28] shows the optimal orbit-to-orbit flight time (that is, the transfer without any constraint on the final polar angle θ) of an ideal sail transfer towards a one-year Type I displaced orbits [32], for a set of three pairs $\{H, \rho\}$. Accordingly, the mathematical model has been adapted to this particular mission scenario by changing the boundary constraints of Eq. (27), that is, the second and the last of Eq. (27) are now replaced with $\lambda_\theta = 0$ and $\mathcal{H}(t_\mathrm{f}) = 1$, respectively.

The simulation results and a comparison with the data obtained from Ref. [28] when $N = 10$, are summarized in Table 1, while the optimal transfer trajectories are shown in Fig. 9.

Hughes and McInnes [28] also show the optimal, ephemeris-constrained transfer to a ESDO with $H = \rho = 0.5$ AU using $N = 10$ control segments and a lightness number $\beta = 0.88$ (i.e., $a_c \simeq 5.2\,\mathrm{mm/s^2}$). In that case, the hybrid numerical technique of Ref. [28] gives an optimal launch date at July 29th 2001 and an arrival date at February 24th 2002, with a flight time of about 210 days. Assuming the same ESDO characteristics, and enforcing the final conditions of Eqs. (27), the proposed approach gives a minimum flight time $t_f = 191$ days, with a difference of about 9%, although such a result has been obtained by neglecting the Earth's orbital eccentricity. The transfer trajectory is drawn in Fig. 10 (which also shows the plane $\mathcal{P}$), while the time-history of the optimal control law is shown in Fig. 11. Note that the functions $\alpha = \alpha(t)$ and $\delta = \delta(t)$, while different from those obtained in

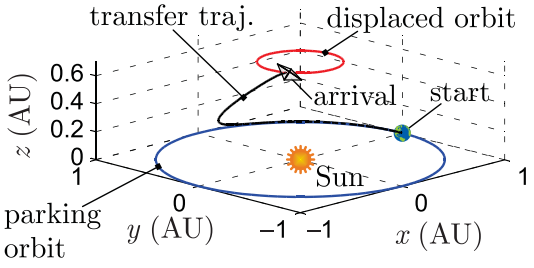

(a) $H = 0.7$ AU and $\rho = 0.3$ AU

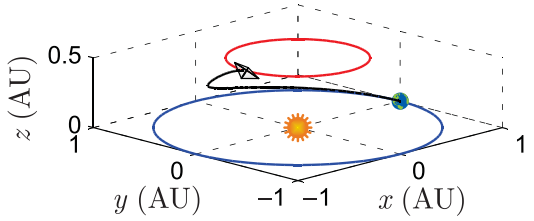

(b) $H = 0.5$ AU and $\rho = 0.5$ AU

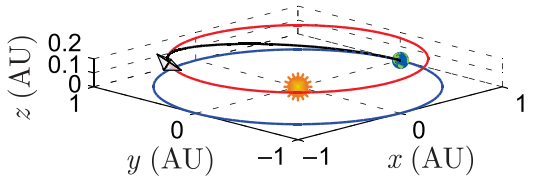

(c) $H = 0.2$ AU and $\rho = 0.9$ AU

Fig. 9 Optimal orbit-to-orbit transfer trajectories for the mission scenarios discussed ($T = 1$ year).

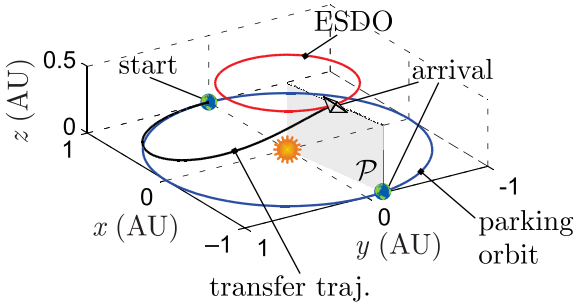

Fig. 10 Optimal transfer trajectory towards an ESDO with $H = \rho = 0.5$ AU.

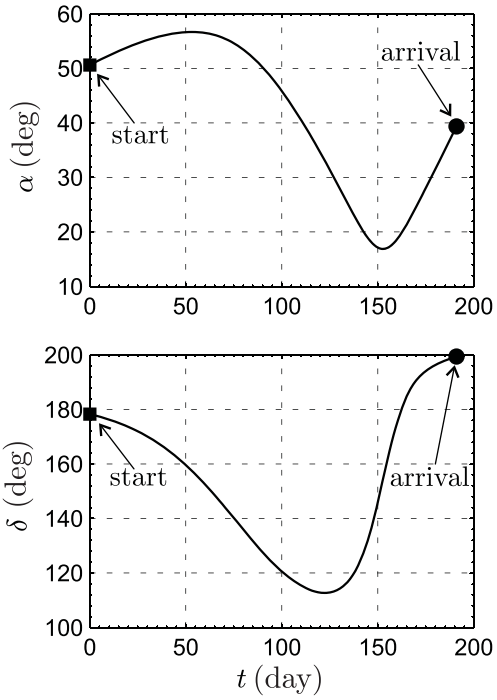

Fig. 11 Optimal control law for a transfer towards an ESDO with $H = \rho = 0.5$ AU.

Ref. [28] using a piecewise-constant steering law with equally-spaced control segments, are however consistent with the results from the literature. In fact, the average values of $\alpha(t)$, corresponding to the first and second half of the whole transfer, approximately coincide with the values of the cone angle shown in Fig. 3 of Ref. [28].

Having validated the mathematical model and the simulation routines, the proposed approach will be used to calculate the minimum flight time of a transfer towards an ESDO with a medium-low performance ideal solar sail. For symmetry reasons, a value of $H > 0$ has been chosen, that is, an ESDO which belongs to the half-space $z > 0$. Using the graphs of Fig. 4(a),

Table 1 Comparison with results obtained in Ref. [28] using a piecewise-constant steering law with $N = 10$ control segments

ESDO characteristics	$H = 0.2$ AU, $\rho = 0.9$ AU	$H = 0.5$ AU, $\rho = 0.5$ AU	$H = 0.7$ AU, $\rho = 0.3$ AU
β	0.4328	0.8808	0.973
a_c (mm/s^2)	2.5665	5.2233	5.7697
t_f (days) from Ref. [28]	158.99	202.71	224.08
t_f (days)	156.46	190.8	211.92
Difference (%)	−1.59	−5.87	−5.42

the optimal value of t_f has been calculated assuming $H \in [0, 0.07]$ AU and $\rho \in [0.94, 1)$ AU. More than 370 optimizations have been performed to numerically obtain the function $t_f = t_f(H, \rho)$ that describes figure of merit of the transfer as a function of the ESDO characteristics. The function $t_f = t_f(H, \rho)$ is shown in Fig. 12, while an excerpt of the numerical results is reported in Table 2.

The use of Fig. 4 and Table 2 allows us to obtain a rapid estimation of the transfer performance for a preliminary mission design. For exemplary purposes, consider an ESDO at a distance from the Earth's center-of-mass of about 0.03 AU $\simeq 4.5 \times 10^6$ km, that is, assume $\widetilde{d} \simeq 0.03$. In that case, Fig. 4(a) indicates that the minimum value of characteristic acceleration necessary to track the ESDO is about $a_{c_d} \simeq 0.4$ mm/s^2. With such a characteristic acceleration, Fig. 4(a) shows that the ESDO displacement is about $H \simeq 0.026$ AU and the radius is $\rho \simeq 0.985$ AU, while Table 2 gives a minimum flight time $t_f \simeq 168$ days. These results are confirmed by the numerical simulations, which give a minimum flight time of 169 days and a transfer trajectory drawn in Fig. 13, where the z-axis has been exaggerated for the sake of clarity.

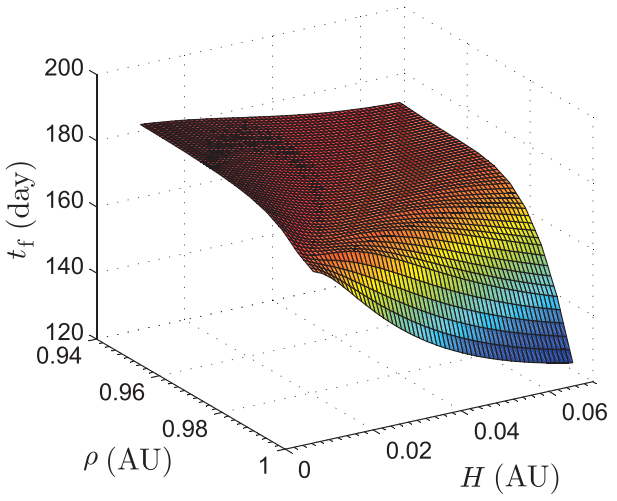

Fig. 12 Minimum flight time as a function of $\{H, \rho\}$.

Table 2 Optimal transfer towards an ESDO for a medium–low performance solar sail: minimum flight time (days) as a function of $\{H, \rho\}$

H (AU) \ ρ (AU)	0.94	0.95	0.96	0.97	0.98	0.99
0.0100	181.97	181.70	181.23	180.25	177.80	170.95
0.0120	181.72	181.35	180.69	179.36	176.23	169.65
0.0140	181.43	180.94	180.08	178.38	174.71	169.02
0.0160	181.11	180.48	179.41	177.36	173.32	168.76
0.0180	180.75	179.99	178.69	176.33	172.14	168.59
0.0200	180.36	179.46	177.95	175.32	171.19	168.32
0.0220	179.95	178.90	177.19	174.37	170.47	167.86
0.0240	179.51	178.32	176.43	173.48	169.97	167.19
0.0260	179.05	177.73	175.69	172.69	169.64	166.32
0.0280	178.58	177.13	174.97	172.01	169.43	165.27
0.0300	178.10	176.54	174.29	171.43	169.32	164.09
0.0320	177.61	175.95	173.65	170.95	169.26	162.81
0.0340	177.13	175.38	173.06	170.58	169.21	161.46
0.0360	176.64	174.83	172.54	170.29	169.15	160.07
0.0380	176.16	174.31	172.07	170.08	169.07	158.66
0.0400	175.69	173.82	171.67	169.94	168.94	157.25
0.0420	175.24	173.36	171.32	169.85	168.76	155.86
0.0440	174.80	172.94	171.04	169.80	168.52	154.49
0.0460	174.38	172.56	170.81	169.77	168.22	153.14
0.0480	173.98	172.21	170.62	169.76	167.87	151.84
0.0500	173.61	171.91	170.48	169.76	167.46	150.57
0.0520	173.27	171.65	170.38	169.75	166.99	149.34
0.0540	172.95	171.43	170.32	169.73	166.48	148.15
0.0560	172.66	171.24	170.28	169.70	165.93	147.00
0.0580	172.40	171.08	170.26	169.65	165.33	145.90
0.0600	172.16	170.96	170.25	169.57	164.71	144.83
0.0620	171.95	170.86	170.26	169.47	164.06	143.81
0.0640	171.78	170.79	170.28	169.34	163.39	142.83
0.0660	171.62	170.75	170.29	169.19	162.70	141.89
0.0680	171.49	170.72	170.31	169.00	161.99	140.98
0.0700	171.39	170.71	170.32	168.79	161.28	140.11

The corresponding time history of the control angles α and δ is shown in Fig. 14, while Fig. 15 shows the time variation of the spacecraft displacement above the ecliptic z and the spacecraft elevation angle γ. Note

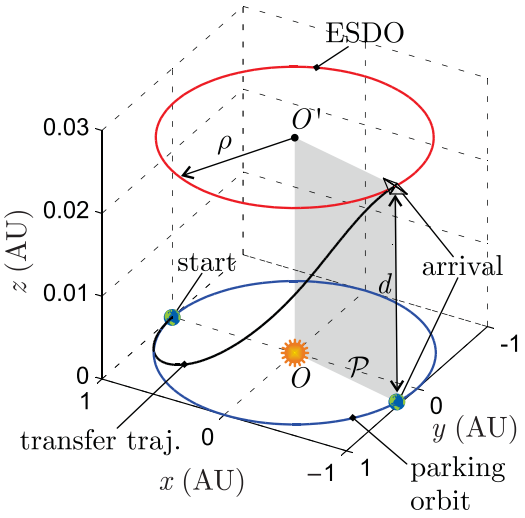

Fig. 13 Optimal transfer trajectory towards an ESDO with $H = 0.026$ AU and $\rho = 0.985$ AU.

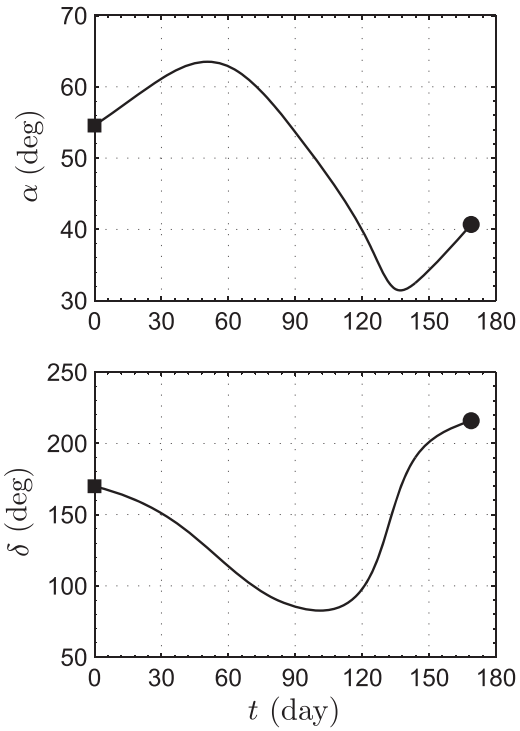

Fig. 14 Optimal control law for a transfer towards an ESDO with $H = 0.026$ AU and $\rho = 0.985$ AU.

that the final value of z matches the constraint $H = 0.026$ AU. Notably, during the transfer the Earth–spacecraft distance is less than 0.03 au, as is confirmed by Fig. 16. This is an important result, because a small Earth–spacecraft distance reduces the complexity of the spacecraft communication subsystem.

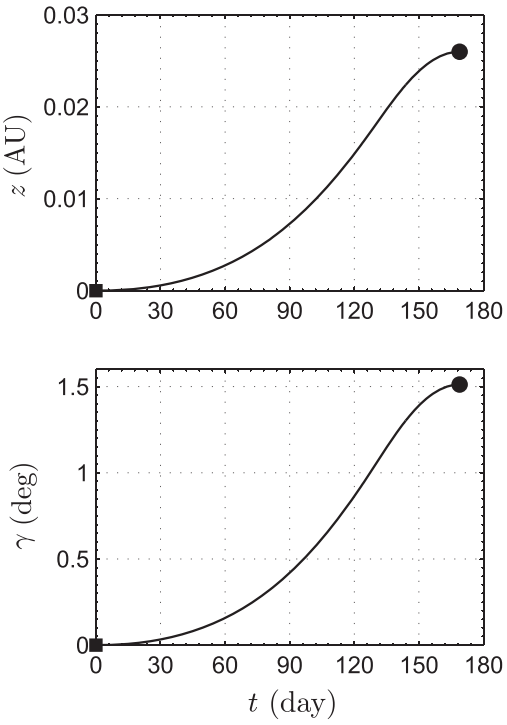

Fig. 15 Spacecraft ecliptic displacement and inclination angle for a transfer towards an ESDO with $H = 0.026$ AU and $\rho = 0.985$ AU.

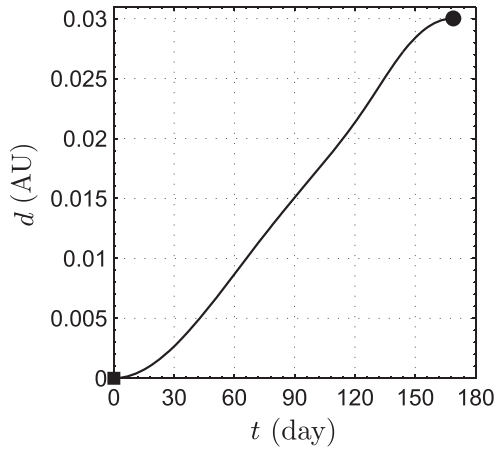

Fig. 16 Time history of Earth-spacecraft distance for a transfer towards an ESDO with $H = 0.026$ AU and $\rho = 0.985$ AU.

4 Conclusions

This paper has presented an optimal approach to calculate the minimum flight time of a solar sail-based spacecraft towards an Earth-synchronous circular displaced orbit. The optimal flight time and the transfer trajectory correspond to a medium–low performance ideal solar sail with a characteristic acceleration sufficient for maintaining the final working orbit. The

optimal solution has been obtained as a function of the orbit radius and displacement of the target Earth-synchronous displaced orbit. The suggested technique shows that the minimum flight time necessary for a transfer from the Earth to the target orbit is less than 182 days when the distance between the two orbits ranges in the interval [0.014, 0.092] AU.

A natural extension of the current analysis may be formulated for heliocentric elliptic displaced orbits, based on the work by Gong and Li [21].

Acknowledgements

This work is supported by the University of Pisa, Progetti di Ricerca di Ateneo (Grant No. PRA_2018_44).

References

[1] McKay, R. J., Macdonald, M., Biggs, J., McInnes, C. Survey of highly non-Keplerian orbits with low-thrust propulsion. *Journal of Guidance, Control, and Dynamics*, **2011**, 34(3): 645–666.

[2] McInnes, C. R. Dynamics, stability, and control of displaced non-Keplerian orbits. *Journal of Guidance, Control, and Dynamics*, **1998**, 21(5): 799–805.

[3] Bookless, J., McInnes, C. Dynamics and control of displaced periodic orbits using solar-sail propulsion. *Journal of Guidance, Control, and Dynamics*, **2006**, 29(3): 527–537.

[4] McInnes, C. R. Displaced non-Keplerian orbits using impulsive thrust. *Celestial Mechanics and Dynamical Astronomy*, **2011**, 110(3): 199–215.

[5] Caruso, A., Mengali, G., Quarta, A. A. Elliptic displaced orbit approximation with equally spaced impulses. *Journal of Guidance, Control, and Dynamics*, **2019**, 42(2): 411–415.

[6] Tsuda, Y., Mori, O., Funase, R., Sawada, H., Yamamoto, T., Saiki, T., Endo, T., Kawaguchi, J. Flight status of IKAROS deep space solar sail demonstrator. *Acta Astronautica*, **2011**, 69(9–10): 833–840.

[7] Johnson, L., Whorton, M., Heaton, A., Pinson, R., Laue, G., Adams, C. NanoSail-D: a solar sail demonstration mission. *Acta Astronautica*, **2011**, 68(5–6): 571–575.

[8] Johnson, L., Young, R., Barnes, N., Friedman, L., Lappas, V., McInnes, C. Solar sails: technology and demonstration status. *International Journal of Aeronautical and Space Sciences*, **2012**, 13(4): 421–427.

[9] Johnson, L., Young, R., Montgomery, E., Alhorn, D. Status of solar sail technology within NASA. *Advances in Space Research*, **2011**, 48(11): 1687–1694.

[10] Janhunen, P., Sandroos, A. Simulation study of solar wind push on a charged wire: basis of solar wind electric sail propulsion. *Annales Geophysicae*, **2007**, 25(3): 755–767.

[11] Mengali, G., Quarta, A. A., Janhunen, P. Electric sail performance analysis. *Journal of Spacecraft and Rockets*, **2008**, 45(1): 122–129.

[12] Ceriotti, M., McInnes, C. R., Diedrich, B. L. The pole-sitter mission concept: An overview of recent developments and possible future applications. In: Proceedings of the 62nd International Astronautical Congress, **2011**: 2543–2559.

[13] Ceriotti, M., Heiligers, J., McInnes, C. R. Trajectory and spacecraft design for a pole-sitter mission. *Journal of Spacecraft and Rockets*, **2014**, 51(1): 311–326.

[14] Ceriotti, M., McInnes, C. R. Natural and sail-displaced doubly-symmetric Lagrange point orbits for polar coverage. *Celestial Mechanics and Dynamical Astronomy*, **2012**, 114(1–2): 151–180.

[15] Heiligers, J., Parker, J. S., Macdonald, M. Novel solar-sail mission concepts for high-latitude earth and lunar observation. *Journal of Guidance, Control, and Dynamics*, **2018**, 41(1): 212–230.

[16] Ozimek, M. T., Grebow, D. J., Howell, K. C. Design of solar sail trajectories with applications to lunar south pole coverage. *Journal of Guidance, Control, and Dynamics*, **2009**, 32(6): 1884–1897.

[17] Wawrzyniak, G. G., Howell, K. C. Investigating the design space for solar sail trajectories in the earth-moon system. *The Open Aerospace Engineering Journal*, **2011**, 4(1): 26–44.

[18] Heiligers, J., Scheeres, D. J. Solar-sail orbital motion about asteroids and binary asteroid systems. *Journal of Guidance, Control, and Dynamics*, **2018**, 41(9): 1947–1962.

[19] Macdonald, M., McKay, R. J., Vasile, M., De Frescheville, F. B., Biggs, J., McInnes, C. Low-thrust-enabled highly-non-Keplerian orbits in support of future Mars exploration. *Journal of Guidance, Control, and Dynamics*, **2011**, 34(5):1396–1411.

[20] West, J. L. The GeoStorm warning mission: enhanced opportunities based on new technology. In: Proceedings of the 14th AAS/AIAA Space Flight Mechanics Conference, **2004**: 29–42.

[21] Gong, S. P., Li, J. F. Solar sail heliocentric elliptic displaced orbits. *Journal of Guidance, Control, and Dynamics*, **2014**, 37(6): 2021–2026.

[22] Gong, S. P., Li, J. F. Spin-stabilized solar sail for displaced solar orbits. *Aerospace Science and Technology*, **2014**, 32(1): 188–199.

[23] Song, M., He, X. S., He, D. S. Displaced orbits for solar sail equipped with reflectance control devices in Hill's restricted three-body problem with oblateness. *Astrophysics and Space Science*, **2016**, 361(10): 327.

[24] Mengali, G., Quarta, A. A. Non-Keplerian orbits for electric sails. *Celestial Mechanics and Dynamical Astronomy*, **2009**, 105(1–3): 179–195.
[25] Niccolai, L., Quarta, A. A., Mengali, G. Electric sail-based displaced orbits with a refined thrust model. *Proceedings of the Institution of Mechanical Engineers, Part G: Journal of Aerospace Engineering*, **2018**, 232(3): 423–432.
[26] Niccolai, L., Quarta, A. A., Mengali, G. Electric sail elliptic displaced orbits with advanced thrust model. *Acta Astronautica*, **2017**, 138: 503–511.
[27] Powers, R. B., Coverstone, V. L. Optimal solar sail orbit transfers to synchronous orbits. *Journal of the Astronautical Sciences*, **2001**, 49(2): 269–281.
[28] Hughes, G. W., McInnes, C. R. Solar sail hybrid trajectory optimization for non-Keplerian orbit transfers. *Journal of Guidance, Control, and Dynamics*, **2002**, 25(3): 602–604.
[29] Mengali, G., Quarta, A. A. Solar sail trajectories with piecewise-constant steering laws. *Aerospace Science and Technology*, **2009**, 13(8): 431–441.
[30] Wright, J. L. *Space Sailing*. Philadelphia: Gordon and Breach Science Publishers, **1992**: 223.
[31] Dachwald, B., Macdonald, M., McInnes, C. R., Mengali, G., Quarta, A. A. Impact of optical degradation on solar sail mission performance. *Journal of Spacecraft and Rockets*, **2007**, 44(4): 740–749.
[32] McInnes, C. R. *Solar Sailing: Technology, Dynamics and Mission Applications*. London: Springer-Verlag Berlin Heidelberg, **1999**: 46–51.
[33] Wie, B. Thrust vector control analysis and design for solar-sail spacecraft. *Journal of Spacecraft and Rockets*, **2007**, 44(3): 545–557.
[34] Aliasi, G., Mengali, G., Quarta, A. A. Artificial Lagrange points for solar sail with electrochromic material panels. *Journal of Guidance, Control, and Dynamics*, **2013**, 36(5): 1544–1550.
[35] Mengali, G., Quarta, A. A. Heliocentric trajectory analysis of sun-pointing smart dust with electrochromic control. *Advances in Space Research*, **2016**, 57(4): 991–1001.
[36] Ceriotti, M., Harkness, P., McRobb, M. Variable-geometry solar sailing: the possibilities of the quasi-rhombic Pyramid. In: *Advances in Solar Sailing*. Macdonlald M., Ed. Berlin, Heidelberg: Spring-Verlag Berlin Heidelberg, **2014**: 899–919.
[37] Heiligers, J., Guerrant, D., Lawrence, D. Exploring the Heliogyro's orbital control capabilities for solar sail halo orbits. *Journal of Guidance, Control, and Dynamics*, **2017**, 40(10): 2569–2586.
[38] Stengel, R. F. *Optimal Control and Estimation*. New York: Dover Publications. **1994**: 222–254.
[39] Sauer, C. G. Jr. Optimum solar-sail interplanetary trajectories. In: Proceedings of the Astrodynamics Conference, **1976**: 792.
[40] Lawden, D. F. *Optimal Trajectories for Space Navigation*. London: Butterworths. **1963**: 54–60.
[41] Mengali, G., Quarta, A. A. Optimal three-dimensional interplanetary rendezvous using non-ideal solar sail. *Journal of Guidance, Control, and Dynamics*, **2005**, 28(1): 173–177.
[42] Niccolai, L., Quarta, A. A., Mengali, G. Analytical solution of the optimal steering law for non-ideal solar sail. *Aerospace Science and Technology*, **2017**, 62: 11–18.
[43] Bryson, A. E., Ho, Y. C. *Applied Optimal Control*. Washington, D. C.: Hemisphere Publishing Corporation. **1975**: 71–89.
[44] Shampine, L. F., Reichelt, M. W. The MATLAB ODE suite. *SIAM Journal on Scientific Computing*, **1997**, 18(1): 1–22.

Alessandro A. Quarta received his Ph.D. degree in aerospace engineering from the University of Pisa in 2005, and is currently a professor of flight mechanics at the Department of Civil and Industrial Engineering of the University of Pisa. His main research areas include spaceflight simulation, spacecraft mission analysis and design, low-thrust trajectory optimization, solar sail and E-sail dynamics and control. E-mail: a.quarta@ing.unipi.it.

Giovanni Mengali received his doctor degree in aeronautical engineering in 1989 from the University of Pisa. Since 1990, he has been with the Department of Aerospace Engineering (now Department of Civil and Industrial Engineering) of the University of Pisa, first as a Ph.D. student, then as an assistant and an associate professor. Currently, he is a professor of space flight mechanics. His main research areas include spacecraft mission analysis, trajectory optimization, solar sails, electric sails and aircraft flight dynamics and control. E-mail: g.mengali@ing.unipi.it.

Marco Bassetto graduated in aerospace engineering in 2016. Since 2016, he is a Ph.D. student at the Department of Civil and Industrial Engineering of the University of Pisa. His research activities mainly focus on mission design and trajectory analysis of spacecraft propelled with low-thrust propulsion systems, such as solar sails and electric solar wind sails. E-mail: marco.bassetto@ing.unipi.it.